Triple oxygen isotope composition of dissolved O_2 in the equatorial Pacific: A tracer of mixing, production, and respiration

Melissa B. Hendricks, Michael L. Bender, and Bruce A. Barnett
Department of Geosciences, Princeton University, Princeton, New Jersey, USA

Peter Strutton[1] and Francisco P. Chavez
Monterey Bay Aquarium Research Institute, Moss Landing, California, USA

Received 30 September 2004; revised 9 June 2005; accepted 27 June 2005; published 20 December 2005.

[1] As a contribution to the study of equatorial Pacific biogeochemistry, we measured the O_2/Ar ratio and the triple isotope composition (^{18}O, ^{17}O, and ^{16}O) of O_2 along six meridional lines in the equatorial Pacific (8°N–8°S at 95°W, 110°W, 125°W, 140°W, 155°W, and 170°W). O_2/Ar ratios and $\delta^{18}O$ were close to equilibrium values within the mixed layer and followed the general trend of increasing $\delta^{18}O$ with decreasing O_2/Ar at greater depths. The $^{17}\Delta$ ($\approx\delta^{17}O-0.5\delta^{18}O$) constrains the fraction of photosynthetic O_2; $^{17}\Delta$ was slightly elevated with respect to equilibrium within the mixed layer due to local photosynthetic production. In aphotic zone waters above 250 m depth the average $^{17}\Delta$ values were higher than in the mixed layer. There are four sources of this photosynthetic signal in the dark ocean: production in the euphotic zone prior to subduction in the distant source regions, production below the mixed layer during travel to the equatorial zone, diapycnal mixing with shallower waters bearing photosynthetic O_2, and accumulation of photosynthetic O_2 produced at very low rates below the 1% light level. Our results also constrain biological production rates within the mixed layer at several locations along 95°W and 110°W. Our average rate of ^{14}C production (53 ± 34 mmol C m^{-2} d^{-1}) agreed well with other estimates in the equatorial Pacific, while our average rate of net C production (6.9 ± 6.2 mmol C m^{-2} d^{-1}) and *f* ratio (0.12 ± 0.11) were somewhat lower than other estimates. Adding $\delta^{18}O$ and $^{17}\Delta$ as tracers to three-dimensional biogeochemical ocean GCMs and comparing results with observations will extend our understanding of metabolic rates in the study region.

Citation: Hendricks, M. B., M. L. Bender, B. A. Barnett, P. Strutton, and F. P. Chavez (2005), Triple oxygen isotope composition of dissolved O_2 in the equatorial Pacific: A tracer of mixing, production, and respiration, *J. Geophys. Res.*, *110*, C12021, doi:10.1029/2004JC002735.

1. Introduction

[2] Two requirements for understanding the biogeochemistry of the Equatorial Pacific are quantifying biological rate processes and building models of circulation and biogeochemistry that correctly simulate various tracer observations. Here we show that variations in the concentration and triple isotopic composition of dissolved O_2 serve as excellent tracers for testing (and possibly improving) both the biological and the circulation aspects of three-dimensional models of the regional biogeochemistry. In addition, they directly constrain gross and net productivity in the surface mixed layer [*Luz and Barkan*, 2000; *Hendricks et al.*, 2004].

[3] The equatorial Pacific is a region of highly diverse ecosystems. There is considerable spatial variability in important production parameters such as temperature and nutrient levels. Researchers have employed a wide array of techniques for studying equatorial Pacific biogeochemistry. Local studies (which have larger-scale implications) include process studies such as patch experiments, incubations that determine ^{14}C and ^{15}N assimilation rates, and species- or community-specific physiological experiments. Expanding in scope, temporal changes in nutrient fields, estimates of dissolved organic carbon and nitrogen concentrations, and measurements of export fluxes with sediment traps are all used to determine seasonal community productivity over spatial scales of tens to hundreds of kilometers. At the largest physical scale, estimates of production are made with ocean color data from satellite images [*McClain et al.*, 2002]. Three-dimensional ocean biogeochemistry models successfully reproduce many of the observations [*Christian et al.*, 2002]. However, the small number of rate observa-

[1]Now at College of Oceanic and Atmospheric Sciences, Oregon State University, Corvallis, Oregon, USA.

0148-0227/05/2004JC002735$09.00

tions against which model predictions can be compared limits our ability to validate models and improve the fidelity of their simulations.

[4] In this study, we present data on the upper water column O_2 concentration and its isotopic composition. We explore, in a qualitative sense, how these properties reflect photosynthesis, respiration, and circulation below the mixed layer. The quantitative interpretation must be made using a 3-D ocean GCM and is beyond the scope of this paper. We also use these data to estimate rates of net and gross production (integrated over the depth of the mixed layer) along 95°W and 110°W [*Luz and Barkan*, 2000].

2. Oxygen Isotope Systematics

[5] We begin with a general discussion of how photosynthesis, respiration, air-sea gas exchange and mixing each affect the concentration and $\delta^{18}O$ of dissolved O_2 ($\delta^{18}_{dis}O$). We then continue with an explanation of how these processes affect the relationship between $\delta^{18}_{dis}O$ and $\delta^{17}_{dis}O$. In this paper, we expand the discussions of *Luz and Barkan* [2000] and *Hendricks et al.* [2004], which focused on O_2 in the mixed layer, to include waters below the mixed layer, where oxygen characteristics serve as tracers of circulation in addition to productivity.

[6] The $\delta^{18}_{dis}O$ covaries with $[O_2]$ in different ways for photosynthesis, respiration, and air-sea gas exchange. (Throughout this paper we use the standard delta notation in units of per mil: $\delta^*O = (X^*/X^*_{std} - 1)10^3$. Here *O is either ^{17}O or ^{18}O and X* is the isotopic ratio ($^*O/^{16}O$) of the sample. X^*_{std} is the isotopic ratio of the standard, which is atmospheric O_2 in this study.) Marine photosynthesis produces O_2 that has the same isotopic composition as seawater [*Guy et al.*, 1993], $\delta^{18}_W O = -22.960‰$. This is $\delta^{18}O$ of Standard Mean Ocean Water (SMOW) with atmospheric O_2 as the standard [*Kroopnick and Craig*, 1972]. Addition of photosynthetic O_2 thus causes an increase in $[O_2]$ and a decrease in $\delta^{18}_{dis}O$.

[7] The $^{18}O/^{16}O$ ratio of O_2 consumed by respiration is lower than the $^{18}O/^{16}O$ ratio of the dissolved O_2. Respiration therefore causes $\delta^{18}_{dis}O$ to rise in the residual dissolved O_2, while it lowers $[O_2]$. When respiration is the only process that affects O_2, $\delta^{18}_{dis}O$ follows a Rayleigh (closed system) distillation curve with a respiratory isotope effect (ε^{18}_R) of approximately 20‰ [*Guy et al.*, 1993; *Kiddon et al.*, 1993]. Mixing, which is, of course ubiquitous, attenuates the $\delta^{18}_{dis}O$ increase with respect to the Rayleigh curve, as $[O_2]$ falls. This effect, explored by *Bender* [1990], *Quay et al.* [1993], and *Levine et al.* [2003], can be understood in terms of a simple thought experiment. Consider a water sample split into two parts. In one part, no O_2 is consumed; in the second, all O_2 is consumed. The waters are recombined with half the original O_2 concentration. The $\delta^{18}O$ of the recombined mixture is identical to the starting value and obviously less than the closed system enrichment at the same O_2 concentration.

[8] The equilibrium $\delta^{18}O$ ($\delta^{18}_{sat}O$) is approximately +0.7‰ at temperatures typical of the surface equatorial Pacific [*Benson and Krause*, 1984; *Kroopnick and Craig*, 1972]. Gas exchange with the atmosphere always pushes $[O_2]$ and $\delta^{18}_{dis}O$ toward the saturation condition; $[O_2]$ and $\delta^{18}_{dis}O$ may either rise or fall, depending on their values with respect to equilibrium.

[9] Next, we discuss the mass-independent anomaly in the isotopic composition of dissolved O_2. During most chemical reactions, the change in $\delta^{17}O$ is approximately equal to 0.5 times the change in $\delta^{18}O$. Therefore, with SMOW as a reference, all O_2 produced by biological processes from ocean water has $\delta^{17}O \sim 0.5\ \delta^{18}O$. Isotope exchange between O_2 and CO_2 in the stratosphere lowers $\delta^{17}O$ and $\delta^{18}O$ of O_2, but not in the 0.5 ratio. In this exchange, $\delta^{17}O$ of O_2 decreases by 1.7 times as much as $\delta^{18}O$ of O_2 decreases, rather than 0.5 times [*Thiemens et al.*, 1991, 1995; *Yung et al.*, 1997; *Luz et al.*, 1999; *Lämmerzahl et al.*, 2002]. This effect produces an anomaly in the isotopic composition of atmospheric O_2: $\delta^{17}_{atm}O$ is less than $0.5\delta^{18}_{atm}O$ by ~0.249‰, with SMOW as the reference [*Luz and Barkan*, 2000].

[10] The quantity $^{17}\Delta$, the most useful measure of this anomaly, is defined by *Angert et al.* [2003] as

$$^{17}\Delta = \left[\ln\left(\delta^{17}O/10^3 + 1\right) - 0.516 \cdot \ln\left(\delta^{18}O/10^3 + 1\right)\right] \cdot 10^6. \quad (1)$$

Here $^{17}\Delta$ is expressed in units of per meg (1 per meg = 0.001‰); 0.516 is the coefficient associated with ordinary dark respiration (cytochrome oxidase pathway [*Angert et al.*, 2003]), assumed here to represent fractionation associated with all O_2 consumption.

[11] For reference, $^{17}\Delta$ can be approximated as $\Delta^{17}O$, when $\delta^{17}O$ and $\delta^{18}O$ are close to zero:

$$^{17}\Delta \sim \Delta^{17}O = \left[\delta^{17}O - 0.516 \cdot \delta^{18}O\right] \cdot 10^3 \quad (2)$$

Since the $\delta^{18}O$ values in our data set range over almost 13‰, we calculate $^{17}\Delta$ from equation (1) instead of its approximation in equation (2).

[12] Marine photosynthesis adds O_2 with $^{17}\Delta_W = +249$ per meg, which is the $^{17}\Delta$ of seawater with respect to atmospheric O_2 [*Luz and Barkan*, 2000]. Thus photosynthesis causes $[O_2]$ and $^{17}\Delta$ of dissolved O_2 ($^{17}\Delta_{dis}$) to rise. Respiration is a mass-dependent process and the change in $\ln(\delta^{17}_{dis}O/10^3 + 1)$ is equal to 0.516 times the change in $\ln(\delta^{18}_{dis}O/10^3 + 1)$. Thus there is no change in $^{17}\Delta_{dis}$ while $[O_2]$ falls due to respiration. Gas exchange again has the effect of forcing O_2 toward equilibrium with the atmosphere. The equilibrium $^{17}\Delta$ of dissolved O_2, $^{17}\Delta_{sat}$, is 16 per meg [*Luz and Barkan*, 2000], and the equilibrium $[O_2]$ is the saturation concentration. Gas exchange will always lower $^{17}\Delta_{dis}$ in waters to which photosynthetic O_2 has been added and leave $^{17}\Delta_{dis}$ unchanged in waters that have no photosynthetic O_2. *Hendricks et al.* [2004] illustrate the direction of changes in $[O_2]$, $\delta^{18}_{dis}O$, and $^{17}\Delta_{dis}$ associated with photosynthesis, respiration, and gas exchange.

[13] As in the work of *Hendricks et al.* [2004], we deal with issues surrounding deviations from saturation caused by physical effects, such as variations in atmospheric pressure, warming, and bubble injection, by measuring the O_2/Ar ratio instead of the O_2 concentration [*Craig and Hayward*, 1987; *Spitzer and Jenkins*, 1989; *Emerson*, 1987; *Quay et al.*, 1993]. O_2 and Ar saturation anomalies are affected similarly by partial air injection from bubbles,

temperature changes, and variations in atmospheric pressure [*Weiss*, 1970; *Craig and Hayward*, 1987]. Since argon has no biological sources or sinks, measurement of argon saturation anomalies are used to remove physical contributions to the oxygen concentration.

[14] For the purpose of calculating $[O_2]$ of our samples when that property was not measured, we assume that [Ar] is at saturation. Any deviations in [Ar] from saturation introduce a small error that does not affect our interpretation. We thus define "biological O_2 saturation" as the O_2/Ar ratio divided by the O_2/Ar ratio at saturation, $([O_2]/[Ar])/([O_2]_{sat}/[Ar]_{sat})$. The denominator is simply a function of temperature and salinity [*Weiss*, 1970]. Then, the "biological O_2 supersaturation" is defined as O_2 supersaturation in excess of Ar supersaturation, and equals the biological O_2 saturation minus one. This approach neglects the fact that complete dissolution of small bubbles injects O_2 and Ar with the air ratio rather than the saturation ratio, a small effect. Deviations in [Ar] from saturation in our samples (likely <2%), introduce a similar error into the calculated values of net and gross production.

3. Methods and Uncertainties

[15] Samples were collected during three different NOAA cruises that serviced buoys of the TAO/TOGA program: (1) a cruise of the R/V *Ron Brown* during November 2000, along 95°W and 110°W, (2) a cruise of the R/V *Ka' imimoana* during February 2001, along 125°W and 140°W, and (3) a cruise of the R/V *Ka' imimoana* during October 2000, along 155°W and 170°W. Along each section, samples were collected at 8°N, 5°N, 2°N, 0°N, 2°S, 5°S, and 8°S, except at 140°W where there was no station at 8°S. Samples were collected from Niskin bottles at depths between 10 and 250 m. We sampled the mixed layer and the thermocline down to an O_2 concentration ~25% of saturation, at which point the concentration is below the level required for triple isotope analyses. Thus maximum sample depths are shallower along the easternmost lines. The equatorial Pacific was not in an El Niño mode at the time of sampling.

[16] For the isotope measurements, approximately 250 mL of water were collected in 500 mL preevacuated bottles that had been poisoned with 75 μL of saturated $HgCl_2$ solution [*Kirkwood*, 1992]. The bottles were constructed and filled as described by *Emerson et al.* [1995]. These samples were prepared and analyzed by mass spectrometry according to the procedure described by *Blunier et al.* [2002] and *Hendricks et al.* [2004]. Briefly, most water was removed from the sample bottle by aspiration. CO_2 and water were removed cryogenically. Noncondensible gases were chromatographed to separate O_2 and Ar from N_2. The O_2 + Ar mixture was analyzed to determine $\delta^{17}O$ and $\delta^{18}O$ of dissolved O_2 and the O_2/Ar ratio.

[17] As will be explained in section 6.1, estimates of net production in the mixed layer are based on the small biological O_2 supersaturation values (typically 1%). Samples from 95°W and 110°W were analyzed within 6 months of collection, with the average period between collection and analysis being 77 days. Storage times were higher for the other samples: the average time between collection and analysis was 627 days for the sections at 125°W and 140°W (the longest time was 720 days), and 505 days for the sections at 155°W and 170°W. Storage tests have documented that, over these timescales, there is significant permeation of O_2 and Ar (M. Reuer, personal communication, 2003). Permeation of O_2 and Ar occurs through the terminal Viton O-ring of the Louwers-Hapert valve, governed by the partial pressure difference across the O-ring, the gas permeability in Viton, and the O-ring geometry. The rate of permeation falls with time. When the valve sidearm is filled with water, as done here, leakage would raise the O_2 content of saturated samples by up to 4% in 627 days, and the most highly undersaturated samples by up to 7% in this time. Permeation would have the effect of lowering $^{17}\Delta$ by about 2 per meg in saturated samples from 125°W and 140°W, and about 8 per meg in highly undersaturated samples. Permeation tests show that the O_2/Ar ratio of air leaking into flasks is close to the atmospheric ratio and about 10% higher than the saturation ratio. Leakage would therefore raise the O_2/Ar ratio of the saturated samples by about 0.4% in samples from 125°W and 140°W, and would raise the O_2/Ar ratio of the most undersaturated samples by up to 5%. Effects were smaller at 155°W and 170°W, and negligible for the two easternmost lines. Because of the possible overestimation of production due to the increased biological O_2 saturation for samples stored for long periods, we elected to calculate productivity values only for mixed layer samples collected along 95°W and 110°W. We have changed our procedures so that samples are now analyzed close to the collection date. Here, we do not make any corrections for the permeation. Uncertainties associated with storage prevent us from calculating mixed layer productivities along the lines from 125°W to 170°W. Otherwise, these uncertainties do not have any influence on the interpretation of the data.

[18] The pairwise agreement of duplicate samples gives another measure of uncertainty. A total of 475 samples were analyzed in this study. Of these, 284 were replicates (142 pairs of samples were analyzed). On average, replicates were measured 102 days apart. Both the mean of each pair and the deviation of each measurement from the mean were calculated. The standard deviation from the mean of all replicates was ±11 per meg for $^{17}\Delta$ (i.e., 68% of sample pairs differ by less than 22 per meg) and ±0.1‰ for $\delta^{18}O$. Precision in $^{17}\Delta$ is poorer than we normally achieve because of the low O_2 content of undersaturated samples. There was no difference in these statistics between the samples analyzed within 6 months of collection and those analyzed after longer storage times.

[19] The overall uncertainty in $^{17}\Delta$ is an order of magnitude smaller than that for $\delta^{17}O$ or $\delta^{18}O$ alone because most error in $\delta^{17}O$ and $\delta^{18}O$ was due to mass-dependent fractionation during sample processing, which has no effect on $^{17}\Delta$. Mass spectrometry contributed ±6 to ±9 per meg (1σ) to the uncertainty in $^{17}\Delta$ of saturated samples, based on variance in individual reference – sample – reference cycles. Sample handling, blank, and other sources contributed a similar amount, ±8 per meg. The two numbers add in quadrature to ±11 per meg. Essentially all uncertainty in $\delta^{18}O$ was from sample handling, as the error introduced by mass spectrometric analysis, ≤0.005‰, was much lower than the overall uncertainty of 0.1‰.

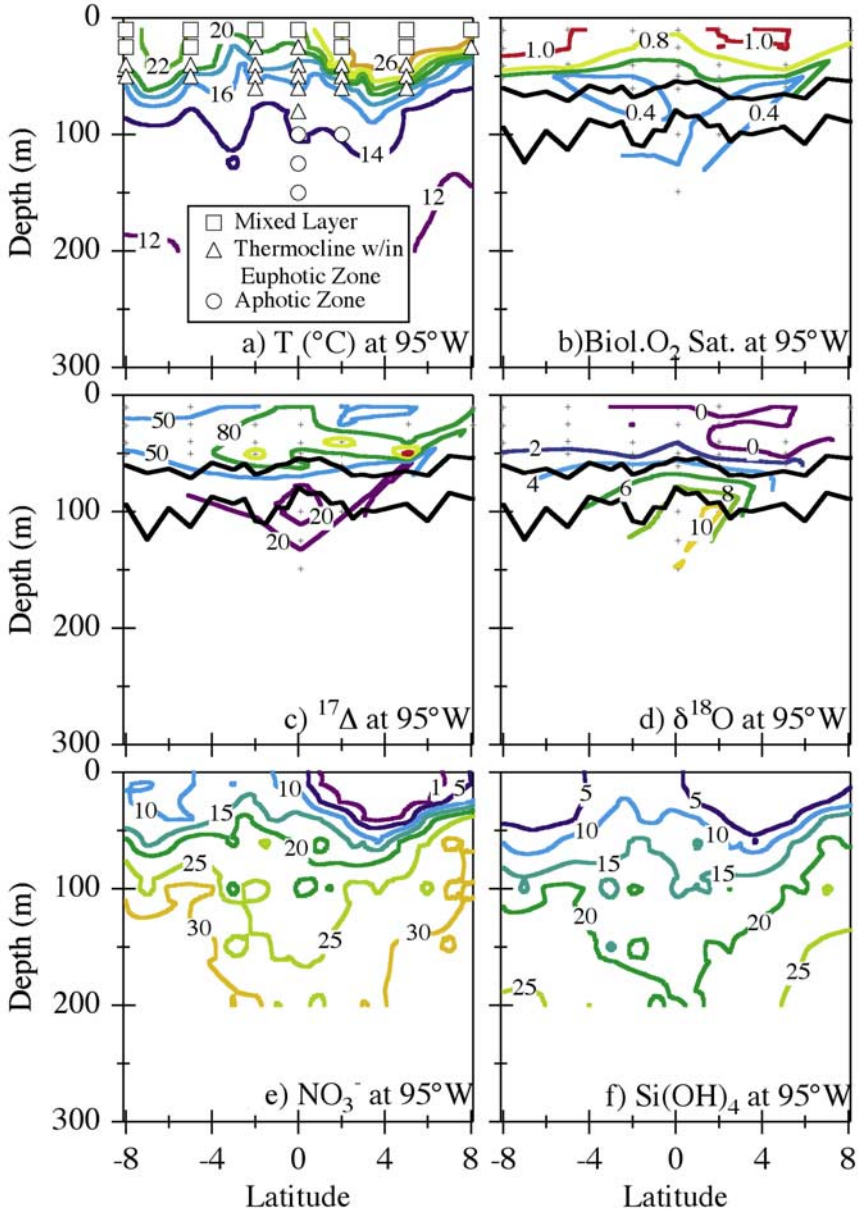

Figure 1. Profiles along 95°W: (a) Temperature (°C), (b) biological O_2 saturation ($\equiv (O_2/Ar)/(O_2/Ar)_{sat}$), (c) $^{17}\Delta_{dis}$ (per meg), (d) $\delta^{18}_{dis}O$(‰), (e) NO_3^- (μmol/L), and (f) $Si(OH)_4$ (μmol/L). Symbols in Figure 1a mark locations of the three water types described in the text: squares, mixed layer; triangles, thermocline within the euphotic zone; circles, aphotic zone. Crosses in Figures 1b, 1c, and 1d mark locations of the O_2 samples used to create the contour plots. The upper and lower subhorizontal lines mark the locations of the 1 and 0.1% light levels, respectively.

[20] We assessed the overall error in the O_2/Ar ratios in a similar fashion, comparison of agreement between replicates. In this case there was a significant difference between samples analyzed within 6 months of collection and those analyzed later. (First we address the error introduced by the mass spectrometer analysis and then move on to discuss the errors introduced through sample preparation and then errors from sample storage and collection.) The standard deviation from the mean of replicate O_2/Ar analyses of our air standard was ±2‰. This was not different from the uncertainty associated with zero enrichments, indicating that the chromatographic separation does not introduce error into the O_2/Ar ratio. The standard deviation from the mean for biological O_2 saturation was again ±2‰ for samples from 95°W and 110°W. The standard deviation from the mean for biological O_2 saturation was ±7‰ for samples from 125°W, 140°W, 155°W, and 170°W, which had longer storage periods.

[21] Temperature profiles were determined from CTD sensors (Figures 1a –6a) [*McTaggart and Johnson*, 2001, 2003]. Water was collected for analysis of nutrients (NO_3^-, PO_4^{3-}, and $Si(OH)_4$), and chlorophyll *a* concentrations from the same Niskin bottles used to collect the samples for isotope measurements (see Figures 1e–6e for $[NO_3^-]$

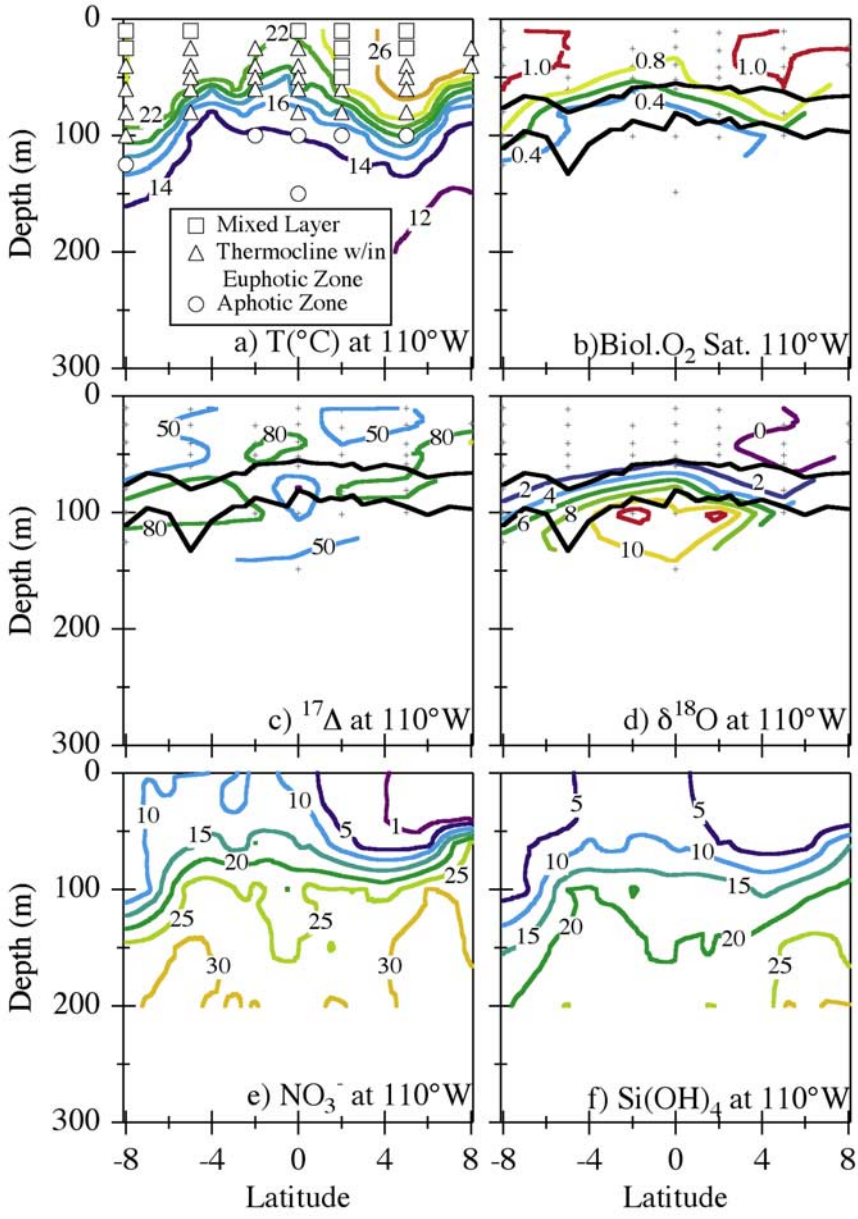

Figure 2. Profiles along 110°W: (a) Temperature (°C), (b) biological O_2 saturation, (c) $^{17}\Delta_{dis}$ (per meg), (d) $\delta^{18}_{dis}O$(‰), (e) NO_3^- (μmol/L), and (f) $Si(OH)_4$ (μmol/L). Symbols and lines are described in Figure 1.

and 1f–6f for [$Si(OH)_4$]). Nutrient samples (10–15 mL) were frozen at −20°C for subsequent analysis at the Monterey Bay Aquarium Research Institute on an Alpkem Rapid Flow Analyzer. Chlorophyll concentration was determined on a Turner 10-005R fluorometer that was calibrated with chlorophyll solutions of known concentration. This is essentially the same method as used by *Chavez et al.* [1996]. The percent surface light as a function of depth was then calculated based on an empirically derived relationship between the attenuation of solar radiation and chlorophyll concentration according to *Morel* [1988].

4. Oxygen Results

4.1. Biological O_2 Saturation

[22] Biological O_2 saturation decreased with depth in the equatorial Pacific (Figures 1b–6b). The waters of the Equatorial Undercurrent (EUC) were clearly identified by the spreading isolines of temperature and biological O_2 saturation near the equator [*Wyrtki and Kilonsky*, 1984; *Archer et al.*, 1996]. In all of the sections, the biological O_2 saturation was less than one in surface waters near the equator. Rates of upwelling are high enough that these waters remain undersaturated as they are advected to the north and south by the Ekman transport until they have spent a sufficient period at the surface to be fully ventilated [*Wanninkhof et al.*, 1995; *Archer et al.*, 1996].

4.2. The $^{17}\Delta$

[23] The overall measured range in $^{17}\Delta_{dis}$ was −25 to +170 per meg (Figures 1c–6c). At all longitudes there was a general trend with depth. Near the surface, gas exchange with the atmosphere maintained relatively low values (close to atmospheric saturation). Below the mixed layer, $^{17}\Delta_{dis}$

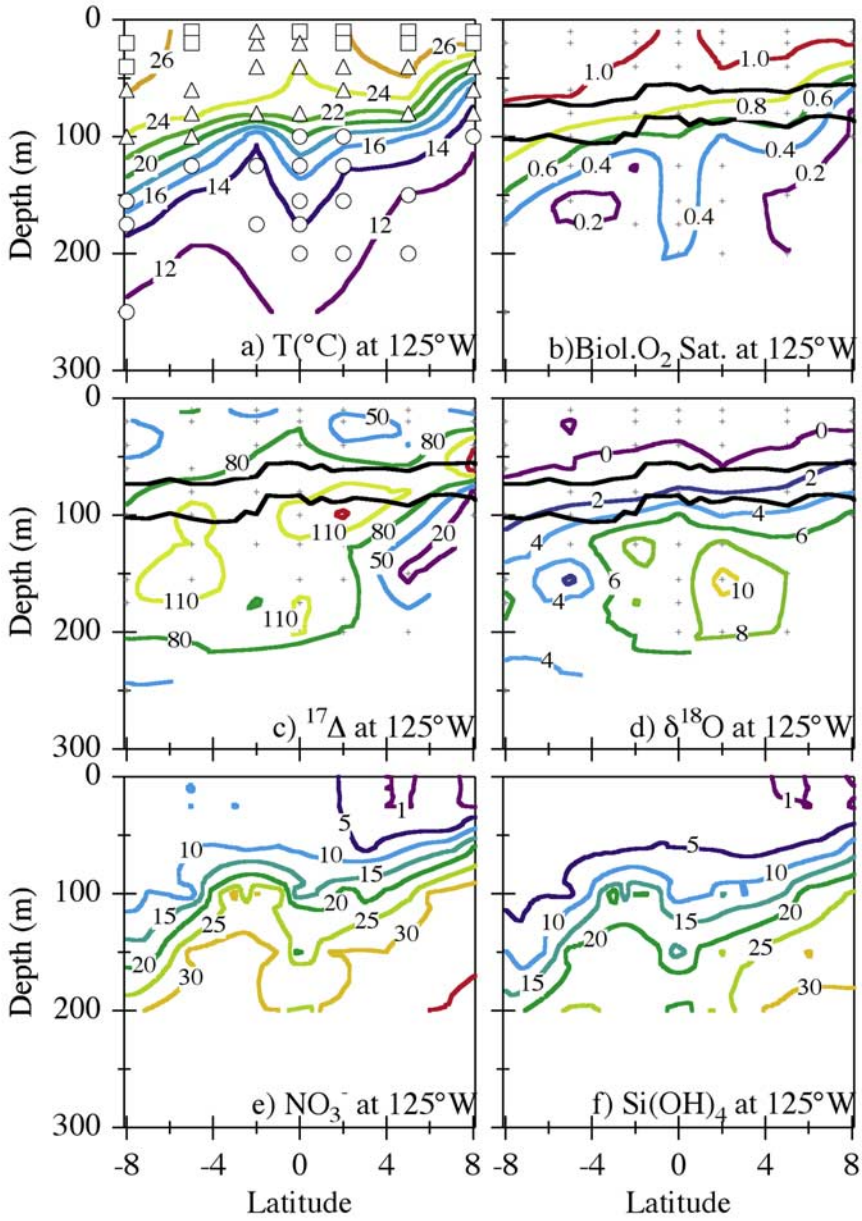

Figure 3. Profiles along 125°W: (a) Temperature (°C), (b) biological O_2 saturation, (c) $^{17}\Delta_{dis}$ (per meg), (d) $\delta^{18}_{dis}O$(‰), (e) NO_3^- (μmol/L), and (f) $Si(OH)_4$ (μmol/L). Symbols and lines are described in Figure 1.

increased to a maximum (reflecting a higher fractional content of photosynthetic O_2) and then decreased again at greater depths. The depth of the $^{17}\Delta_{dis}$ maximum was generally above the 0.1% light level at 95°W and 110°W. West of 110°W, the maximum $^{17}\Delta_{dis}$ values, and hence the greatest fractional content of photosynthetic O_2, were below the 0.1% light level.

[24] The lowest possible $^{17}\Delta_{dis}$ value for our samples is +16 per meg, corresponding to atmospheric equilibrium according to *Luz and Barkan* [2000]. The 8 samples with measured values that fell below this limit were mostly within 1σ uncertainty of +16 per meg and are discussed in detail in section 5.2. These outliers were from deeper waters (low photosynthetic O_2 content) that were highly undersaturated in O_2 and hence had larger mass spectrometer uncertainties.

4.3. The $\delta^{18}_{dis}O$

[25] The range in $\delta^{18}_{dis}O$ was −1.4 to +13.2‰ (Figures 1d–6d). Gas exchange forces the $\delta^{18}_{dis}O$ of surface O_2 toward the equilibrium condition of +0.7‰ [*Kroopnick and Craig*, 1972; *Benson and Krause*, 1984]. Lowest values are found within the euphotic zone, where addition of photosynthetic O_2 lowers $\delta^{18}_{dis}O$. Generally, $\delta^{18}_{dis}O$ increases and biological O_2 saturation decreases with depth because respiration discriminates against the heavy isotope [*Kroopnick and Craig*, 1976; *Quay et al.*, 1993; *Levine et al.*, 2003], and our samples mostly followed this pattern. However, some

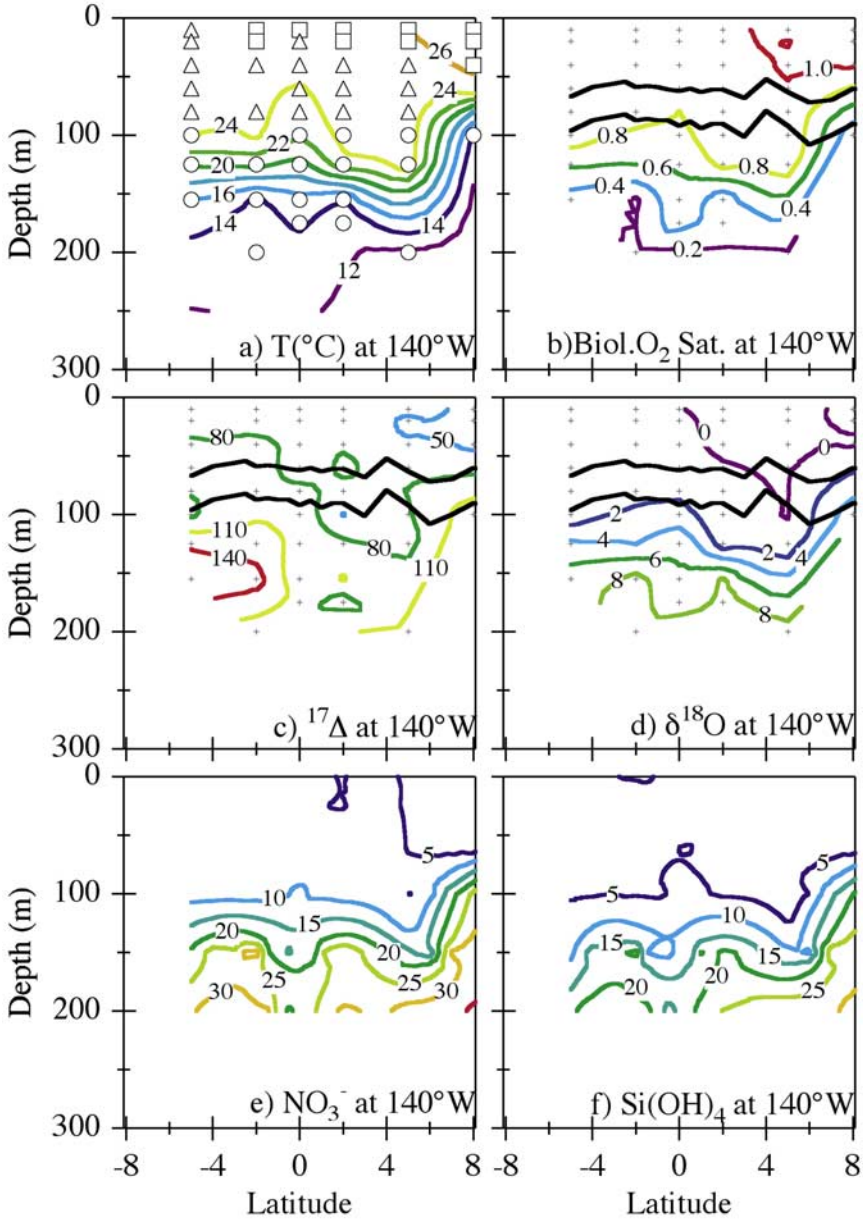

Figure 4. Profiles along 140°W: (a) Temperature (°C), (b) biological O_2 saturation, (c) $^{17}\Delta_{dis}$ (per meg), (d) $\delta^{18}_{dis}O$(‰), (e) NO_3^- (μmol/L), and (f) $Si(OH)_4$ (μmol/L). Symbols and lines are described in Figure 1.

highly undersaturated samples had little or no $\delta^{18}O$ enrichment; we discuss this interesting result below.

5. O_2 Isotopic Properties as Tracers of Circulation and Mixing

[26] In this section we examine the O_2 concentration and isotope systematics in simple qualitative models, thereby demonstrating the potential for using these properties as tracers of both mixing and biology in the equatorial Pacific. We consider three water domains: (1) the aphotic zone, (2) the thermocline within the euphotic zone, and (3) the mixed layer. We show how samples from this study fit into each category and how the O_2 systematics of each category are distinctive. We begin this discussion with a general description of circulation in the equatorial Pacific followed by the criteria used to group the sample locations. Then, each water mass type is examined.

[27] The zonal current system determines general patterns of temperature, nutrient, and O_2 concentrations. Along the equator, isolines of physical, chemical, and biological properties (temperature, nutrients, and chlorophyll) shoal to the east as the core of the Equatorial Undercurrent (EUC) rises from west to east. In the eastern Pacific the EUC splits into several branches, at least one of which enters the South Equatorial Current (SEC), which travels to the west. Phytoplankton production removes nutrients in the SEC, so that there is a clear decrease in $Si(OH)_4$, NO_3^-, and PO_4^{3-} concentrations to the west.

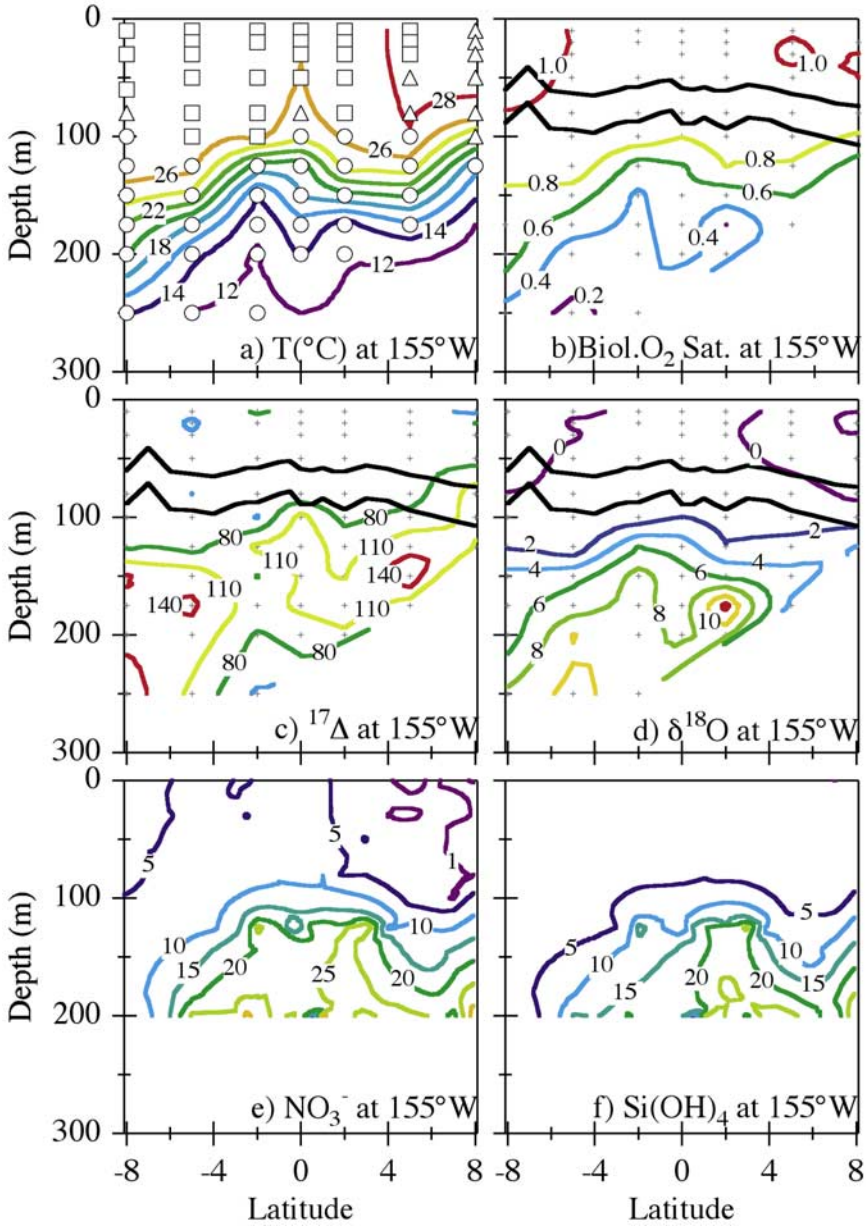

Figure 5. Profiles along 155°W: (a) Temperature (°C), (b) biological O_2 saturation, (c) $^{17}\Delta_{dis}$ (per meg), (d) $\delta^{18}_{dis}O$(‰), (e) NO_3^- (μmol/L), and (f) $Si(OH)_4$ (μmol/L). Symbols and lines are described in Figure 1.

[28] Characteristics of the zonal currents are evident in the meridional sections (Figures 1–6). The EUC is clearly visible in the temperature and biological O_2 saturation profiles as spreading of the isolines at the equator. The shoaling in low-temperature, high-nutrient waters near 8°N is due to the divergent Ekman flow at the boundary between the eastward flowing North Equatorial Countercurrent (NECC) and the westward flowing North Equatorial Current (NEC) [*Wyrtki and Kilonsky*, 1984].

[29] Elements of the meridional circulation cells are manifested in these profiles as well. In general, waters upwell in a very narrow band near the equator, and spread along the surface to the north and south. Shoaling of isolines (temperature, nutrients, biological parameters) is evident between 2°S and the equator. Solar energy warms these waters and phytoplankton production depletes surface nutrients. Thus temperatures increase and nutrients decrease away from the equator. The export of water along the surface is counterbalanced by return flow to the equator through the main thermocline and by upwelling of the EUC. The trough in temperature and nutrients near 4°N is evidence of downwelling into the thermocline associated with the NECC [*Philander et al.*, 1987].

[30] In Figures 1a –6a we characterized samples according to domain. Circles, triangles, and squares represent the aphotic zone, the thermocline within the euphotic zone, and the surface mixed layer, respectively. We define the aphotic zone as the region below the 0.1% light level. To start, we assume that these waters are ventilated (saturated) in a deep wintertime mixed layer in areas of the subtropics and travel

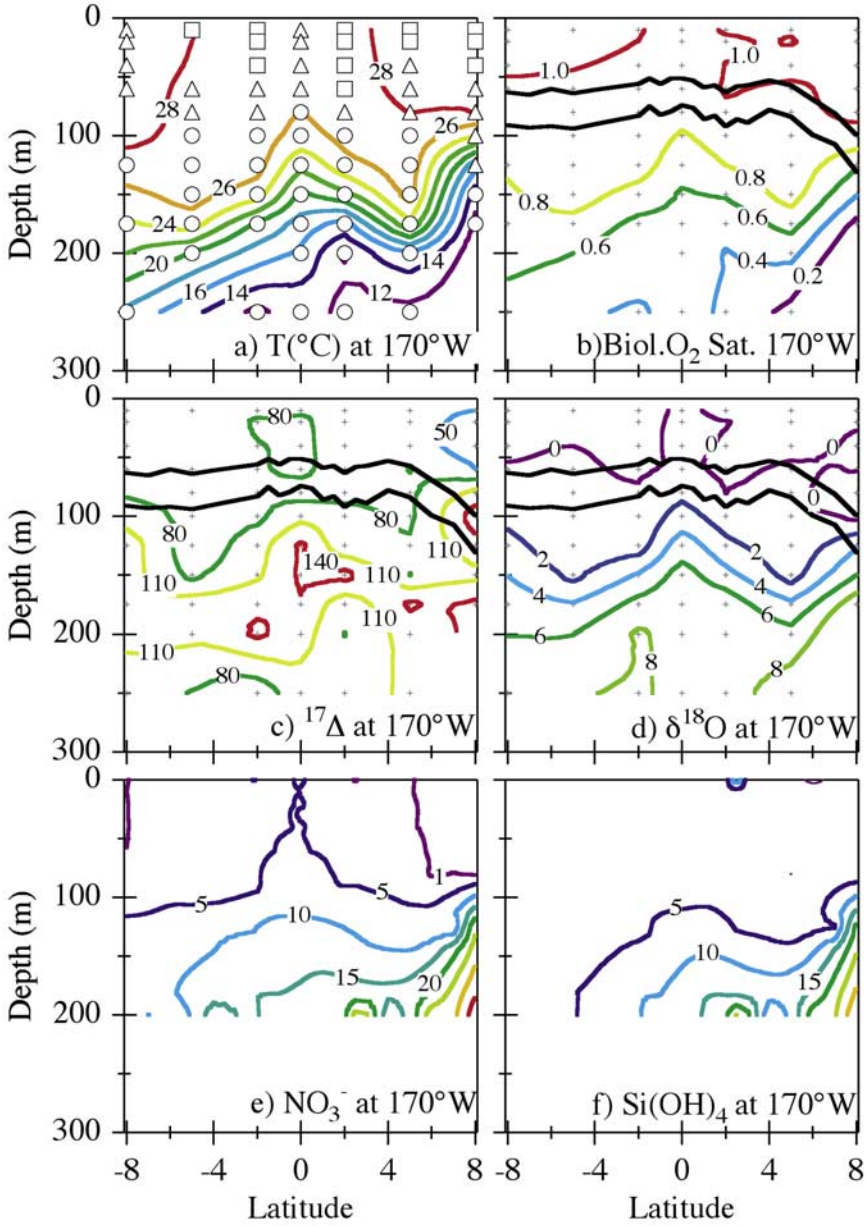

Figure 6. Profiles along 170°W: (a) Temperature (°C), (b) biological O_2 saturation, (c) $^{17}\Delta_{dis}$ (per meg), (d) $\delta^{18}_{dis}O$(‰), (e) NO_3^- (μmol/L), and (f) $Si(OH)_4$ (μmol/L). Symbols and lines are described in Figure 1.

below the mixed layer to reach the equatorial region. In this situation, respiration rates determine $\delta^{18}_{dis}O$ and biological O_2 saturation. The $^{17}\Delta_{dis}$ serves to integrate the total photosynthetic production along this path, as will be explained in section 5.1.

[31] The thermocline within the euphotic zone (triangles in Figures 1a–6a) is defined as the depth interval between the mixed layer and the 0.1% light level. In this region, both photosynthesis and respiration affect O_2 properties. Gas exchange occurs only at the surface outcrop of these waters.

[32] The mixed layer (squares in Figures 1a–6a) is defined as waters above the depth where the density first exceeds the surface density by 0.03 kg m^{-3} [*Gardner et al.*, 1995]. On the basis of this criterion the depth of the mixed layer at our sample stations ranged between 10 and 100 m, similar to the results of *Gardner et al.* [1995] and *Ando and McPhaden* [1997]. We note that there is chemical evidence for stratification within the mixed layer as it is defined here (e.g., Figure 5). In this layer, air-sea gas exchange, photosynthesis, and respiration all play roles in setting the O_2 properties.

5.1. Aphotic Zone

[33] Waters in the aphotic zone (open circles in Figures 1a–6a, 7a, and 7b) are subject to respiratory O_2 consumption after being isolated below the mixed layer. These samples were undersaturated in O_2, but some were very close to saturation, presumably due to deep mixed layers and recent ventilation. The general trend of increasing $\delta^{18}_{dis}O$ with decreasing biological O_2 saturation

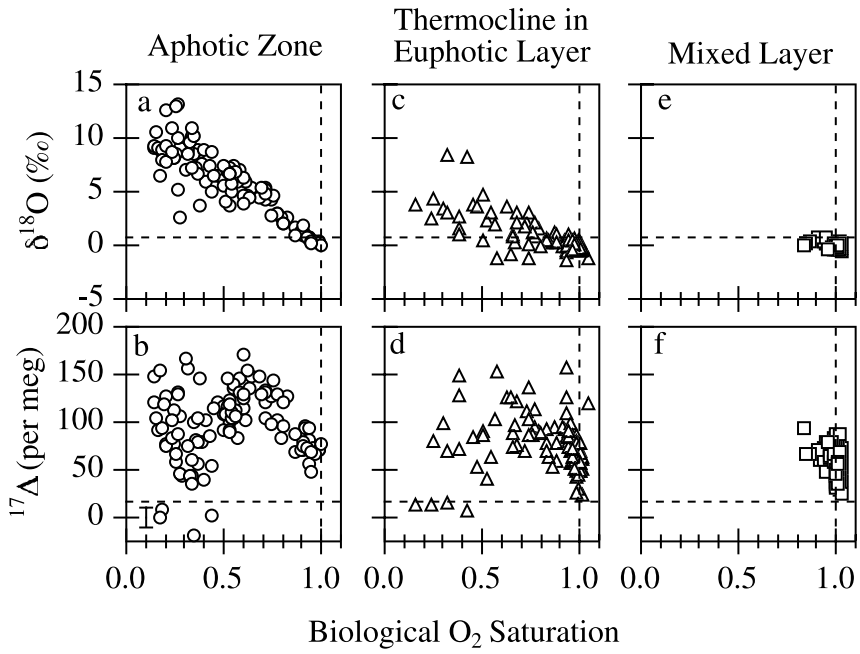

Figure 7. Plots showing (top) $\delta_{dis}{}^{18}O$(‰) and (bottom) $^{17}\Delta_{dis}$ (per meg) versus biological O_2 saturation for the three water types: (a and b) the aphotic zone, (c and d) the thermocline within the euphotic zone, and (e and f) the mixed layer. A representative error bar for $^{17}\Delta_{dis}$ (±11 per meg) is shown in Figure 7b. Errors in $\delta_{dis}{}^{18}O$(±0.1‰) and biological O_2 saturation (±0.002 at 95°–110°W and ±0.007 at other locations) are smaller than the size of the symbols.

(Figure 7a) fits the common relationship found in aphotic zone waters due to discrimination against the heavy isotope by respiration. In aphotic waters of the equatorial Pacific, as elsewhere, $\delta^{18}O$ rose roughly linearly, from +0.7 to ~13‰, as biological O_2 saturation fell from 1 toward 0 [*Kroopnick and Craig*, 1976; *Bender*, 1990; *Levine et al.*, 2003].

[34] The other isotopic property, $^{17}\Delta_{dis}$, displayed a more complex pattern with biological O_2 saturation (Figure 7b). The shallowest samples had the highest values of biological O_2 saturation (greater than ~0.85). In these samples, $^{17}\Delta_{dis}$ was between 40 and 100 per meg, indicating the presence of significant amounts of biologically produced O_2. At lower biological O_2 saturations, $^{17}\Delta_{dis}$ actually increased, to 100–175 per meg. This increase indicates that the fractional contribution of photosynthetic O_2 rose, in these dark waters, as $[O_2]$ fell. As biological O_2 saturation dropped to values below 0.6, the maximum $^{17}\Delta_{dis}$ remained as high as 170 per meg while the minimum decreased to values within the uncertainty of saturation (See the next section for a discussion of the four points below the saturation value.). Thus, in waters between the 0.1% light level and the O_2 minimum of the equatorial Pacific, 50% or more of the dissolved O_2 can come from photosynthesis (50% corresponds to $^{17}\Delta_{dis}$ = 132.5 per meg). In addition to diapycnal mixing, three processes are likely responsible for this high inventory of photosynthetic O_2: 1) biological production in the stratified euphotic zone of the source regions prior to subduction, 2) production below the mixed layer as waters travel to the equator, and possibly 3) low rates of local photosynthetic activity below the 0.1% light level. We examine each process in turn.

[35] Shallow thermocline waters in the equatorial Pacific are ventilated and leave the mixed layer in large areas of the subtropics [*Gu and Philander*, 1997; *Harper*, 2000; *Rodgers et al.*, 2003]. When the waters are first entrained, they would have a slightly elevated $^{17}\Delta_{dis}$ that reflects the relative rates of photosynthesis and gas exchange in the mixed layer. In the second, related, process, $^{17}\Delta_{dis}$ increases due to photosynthesis in the lower (stratified) euphotic zone as waters travel toward the equator. These waters are isolated from exchange with the atmosphere, and the $^{17}\Delta_{dis}$ signal accumulates. Even in waters that are net heterotrophic, when respiration rates exceed gross production rates (and biological O_2 saturation decreases), $^{17}\Delta_{dis}$ rises because its value is unaffected by respiration, a mass-dependent process.

[36] The third process, local photosynthetic production, could also contribute to increased $^{17}\Delta_{dis}$. Even though these waters are below the 0.1% light level, they do contain measurable levels of chlorophyll (<0.20 μg/L). Analysis of ^{14}C-based productivity data from other cruises along 155°W and 170°W indicates that productivity at the 1% and 0.1% light levels is up to 5% and 1%, respectively, of the near-surface productivity. Since O_2 levels in these waters are low, even small additions of photosynthetic O_2 (with $^{17}\Delta$ = 249 per meg) can cause $^{17}\Delta_{dis}$ to increase. As well, the relatively long residence times of the deeper waters studied here allow inventories of $^{17}\Delta_{dis}$ to grow even when photosynthetic O_2 fluxes are small. Evidence for in situ photosynthesis below the 0.1% light level comes from the fact that $^{17}\Delta_{dis}$ is frequently at a maximum in this zone, and it is not clear that the high $^{17}\Delta_{dis}$ values can derive from higher latitudes or zonal flows (e.g., 170°W transect,

Figure 6). The possibility of small but significant rates of photosynthesis below the 0.1% light level needs to be investigated further.

5.2. Thermocline Within the Euphotic Zone

[37] Samples in the second group were from waters below the base of the mixed layer and above the 0.1% light level (triangles in Figure 1a–6a). In this region, there is enough light to promote higher rates of photosynthetic O_2 production. As in all regions, respiration consumes O_2. Waters in this group are isolated from air-sea gas exchange, except in locations like 2°S and the equator where the thermocline outcrops at the surface.

[38] Biological O_2 saturation in our samples of sunlit, stratified waters ranged from 0.167 to 1.044 (Figures 7c and 7d), and decreased with depth (Figures 1d–6d). Most samples were net heterotrophic (biological O_2 saturation < 1) because of low irradiance. Nevertheless, high $^{17}\Delta$ values signify that photosynthesis was actively cooccurring with respiration.

[39] At biological O_2 saturation less than ~0.8, $\delta^{18}_{dis}O$ tended to be lower than in the aphotic zone, while $^{17}\Delta_{dis}$ of the two water masses is similar (Figure 7). The low $\delta^{18}_{dis}O$ values result from the effect of photosynthetic O_2 addition in the absence of air-sea gas exchange. Waters that upwell from the aphotic zone are undersaturated in O_2. Because $[O_2]$ is low, addition of photosynthetic O_2 ($\delta^{18}_{dis}O \sim -23‰$), or mixing of surface waters with $\delta^{18}_{dis}O$ closer to the equilibrium value of 0.7‰, leads to substantial decreases in $\delta^{18}_{dis}O$, without causing high O_2 concentrations. The $^{17}\Delta_{dis}$ is less affected because addition of photosynthetic O_2(= +249 per meg) and mixing from above (+20 to +95 per meg; see section 5.3) tend to have opposite effects, and maintain $^{17}\Delta_{dis}$ at some intermediate value.

[40] The 8 samples in Figures 7b and 7d that fall below $^{17}\Delta_{dis}$ = 16 per meg (the saturation value) merit further discussion. With the exception of one point, these samples are within the uncertainty of the saturation value. One possible explanation for the low values is contamination with atmospheric air during sample collection or storage. This explanation is unlikely for three reasons. First, the $\delta^{18}_{dis}O$ of these samples is elevated with respect to atmospheric O_2. 6 of the 8 samples have $\delta^{18}_{dis}O$ between 6.4‰ and 10.1‰ and the other two have $\delta^{18}_{dis}O$ of 2.5‰ and 3.9‰. If the samples were contaminated with atmospheric O_2, we would expect the measured $\delta^{18}_{dis}O$ to be closer to 0.8‰. Second, the 8 samples were from locations along 95°W, 110°W, and 125°W. Samples collected from the western 3 lines (140°W, 155°W, and 170°W) were generally stored for a longer period of time before analysis and had the lowest biological O_2 saturations. Thus samples from the western sections would more likely be affected by contamination during storage.

[41] Finally, we see in Figures 1c, 2c, and 3c that the samples affected (outlined by the 20 per meg contour; note the sample at 110°W, 0°N, 80m) were collected from proximal locations at the equator or north of the equator. Contamination should affect low O_2 samples from all latitudes equally and we would expect to find some of these unusual $^{17}\Delta_{dis}$ values at locations south of the equator. Because the number of samples is small and their locations tend to be along or near the edges of our sampling area, we feel speculation about the sources of these low $^{17}\Delta_{dis}$ values would be premature at this time. More observations and incorporation of O_2 isotopes in biogeochemical models of the equatorial Pacific and its sources are necessary to further investigate these results.

5.3. Mixed Layer

[42] In the mixed layer (squares in Figures 1a–6a), a balance of air-sea gas exchange, respiration, and photosynthesis determines the O_2 properties (Figures 7e and 7f). Samples within the equatorial upwelling were undersaturated in O_2 because upwelled waters have not yet been ventilated, and the contribution from photosynthesis is still small because of the relatively brief exposure to light. In samples away from the equator, however, biological O_2 saturation and $\delta^{18}_{dis}O$ were close to the equilibrium point (biological O_2 saturation = 1 and $\delta^{18}_{dis}O$ = +0.7‰) for two reasons. First, ratios of net to gross production are low [e.g., *Fiedler et al.*, 1991; *Chavez et al.*, 1996; *McCarthy et al.*, 1996] (also see section 6.3) because of efficient recycling of nutrients associated with limitation by iron [*Coale et al.*, 1996] and perhaps silicate [*Dugdale and Wilkerson*, 1998]. Respiration causes $\delta^{18}_{dis}O$ to rise, counteracting the $\delta^{18}_{dis}O$ lowering caused by photosynthetic O_2 addition. Second, rates of gas exchange are relatively high, driving $[O_2]$ and $\delta^{18}_{dis}O$ toward atmospheric equilibrium. At all locations within the mixed layer, $^{17}\Delta_{dis}$(= 24 to 94 per meg) was elevated with respect to atmospheric equilibrium, because of photosynthesis. Gas exchange attenuates this increase in $^{17}\Delta_{dis}$. The mixed layer $^{17}\Delta_{dis}$ signal was less than in the stratified euphotic zone or aphotic zone due to the relative rates of gas exchange and photosynthesis. Relatively high rates of photosynthesis and gas exchange in the mixed layer yield low to moderate $^{17}\Delta_{dis}$ values; diminished photosynthesis rates with no gas exchange below the mixed layer generate high $^{17}\Delta_{dis}$ values.

[43] On the equator, biological O_2 saturation was less than zero because upwelling waters have a history of net heterotrophy. The $\delta^{18}_{dis}O$ was somewhat elevated because respiration discriminates against the heavy isotope of O_2. The $^{17}\Delta_{dis}$ was also elevated, for two reasons. First, samples retain a memory of earlier photosynthesis that has not yet been dissipated by gas exchange. Second, equatorial waters are the most nutrient-rich, hence have the highest rates of gross production in the region.

6. Net and Gross Production Rates in the Mixed Layer

[44] In this section, we estimate rates of net O_2 production, gross O_2 production, and ratios of net to gross O_2 production at sampling locations along 95°W and 110°W. As described in section 3, samples from the other transects suffer from possible storage effects and cannot be interpreted in this way. We approximate the mixed layer O_2 balance as a steady state situation, where rates of photosynthesis, respiration and gas exchange are constant and O_2 characteristics do not change with time.

[45] This model ignores the effects of horizontal transport, both surface flow from east to west across the basin and transport away from the equator to the north and south. However, this method of estimating production rates relies

on an O_2 signal that is integrated over a timescale of 7–10 days, and therefore reflects production along the recent flow path of waters we sampled. As we discuss in section 6.2, we can apply our method only well to the north and south of the equatorial upwelling, where waters have lost their memory of initial O_2 undersaturation. Along 95°W and 110°W, maximum zonal velocities, above 50 m depth, occur along the equator, where they are <0.5 m s^{-1} [*Johnson et al.*, 2002], an advection rate of less than 3° longitude per week. Considering this transport rate, O_2 properties at the equator are likely representative of waters within 5° to the east. At the locations where we determined productivity estimates, advection rates are lower, and our rates represent productivities within a few degrees of the collection site. Since there is little zonal variation in equatorial chlorophyll levels, west of 85°W [*McClain et al.*, 2002], we do not believe that zonal advection within the mixed layer aliases our productivity estimates at 95°W and 110°W.

[46] In section 6.1 we explain the methods used for calculating the rates of production based on this steady state approach. Because of intense upwelling, this particular mixed layer model is inappropriate near the equator. In section 6.2 we describe a simple model of upwelling that demonstrates how the O_2 concentration increases and the isotopic composition evolves under conditions of constant gross and net O_2 production after waters reach the surface. On the basis of this model and the data, we restrict the samples used for the production estimates to those away from the upwelling center, where the model predicts O_2 properties approach steady state. In section 6.3 we show the results of our production rate calculations and compare our results to others. Our estimate for the community respiration fractionation factor is described in section 6.4.

6.1. Steady State Model

[47] We rely on a steady state model of O_2 and its isotopes in the surface mixed layer [*Emerson*, 1987; *Quay et al.*, 1993; *Luz and Barkan*, 2000]. We assume no mixing across the base of the mixed layer, and neglect horizontal advection and mixing. The specific equations we use to calculate biological production rates are derived in the appendix of *Hendricks et al.* [2004] and will not be reproduced here.

[48] In the absence of exchange with underlying waters, the O_2 concentration is determined by the relative strengths of photosynthesis, respiration, and gas exchange [*Emerson*, 1987]:

$$h\frac{dC}{dt} = G - R + k(C_{sat} - C) = N + k(C_{sat} - C) \qquad (3)$$

where h is the depth of the mixed layer in meters and C is the O_2 concentration in mmol O_2 m^{-3}. G, R, and N are the rates of gross photosynthetic production, respiration, and net production, respectively, integrated over the depth of the mixed layer (mmol O_2 m^{-2} d^{-1}). k is the gas exchange coefficient for O_2 (m d^{-1}), and C_{sat} is the surface saturation O_2 concentration. The product kC_{sat} is the gross rate of O_2 invasion from the atmosphere and kC is the gross rate of O_2 evasion to the atmosphere. Thus the term $k(C_{sat} - C)$ is the net rate of air-sea gas exchange.

[49] At steady state dC/dt = 0, and the rate of net O_2 production is determined from measurements of the biological O_2 saturation (which we equate with the ratio C/C_{sat}) and the gas exchange coefficient, k [*Spitzer and Jenkins*, 1989; *Emerson*, 1987; *Emerson et al.*, 1993]. k was calculated using the wind speed parameterization of *Wanninkhof* [1992], and the average wind speeds at each location from NCEP reanalysis 10 m wind speeds (NCEP reanalysis data provided by the NOAA-CIRES Climate Diagnostics Center, Boulder, Colorado, USA, http://www.cdc.noaa.gov/). The appropriate period over which to average is the residence time of O_2 in the mixed layer due only to exchange with the atmosphere. The residence time depends on both the gas exchange rate and the depth of the mixed layer (residence time = h/k). At each location, k was determined through an iterative process that accounted for the local wind speed history, albeit in a highly simplified way. The O_2 residence time was calculated given the mixed layer depth and gas exchange coefficient for the 24 hours prior to the sample collection. This process was repeated over longer periods (increasing by 1 day) until the calculated residence time agreed with the averaging period. k ranged between 1.6 and 8.2 m d^{-1}.

[50] Gross production rates and net to gross ratios are constrained by $^{17}\Delta_{dis}$. To calculate gross production rates, we begin with analogs to equation (3) for the three isotopomers and express $\delta^{17}_{dis}O$ and $\delta^{18}_{dis}O$ in terms of the ratio of gross production rate to the rate of gas invasion (G/kC_{sat}), the biological O_2 saturation (C/C_{sat}), and the community respiration fractionation factor (α^*_R) [*Hendricks et al.*, 2004, equation (2)]. To estimate N/G ratios, we substitute $N/(C/C_{sat} - 1)$ for kC_{sat} (see equation (3)) to express $\delta^{17}_{dis}O$ and $\delta^{18}_{dis}O$ in terms of N/G, C/C_{sat}, and α^*_R [*Hendricks et al.*, 2004, equation (3)]. The formal expressions for $^{17}\Delta_{dis}$ in terms of these properties follow by substituting these equations in the definition, $^{17}\Delta/10^6 = \ln(\delta^{17}O/10^3 + 1) - 0.516 \ln(\delta^{18}O/10^3 + 1)$. We solve for G/kC_{sat} and N/G through an iterative process. G is then determined by multiplying G/kC_{sat} by the site-specific value for kC_{sat}.

[51] In principle, gross O_2 production can be calculated from $\delta^{18}_{dis}O$ (or $\delta^{17}_{dis}O$) alone. In practice, this approach fails due to uncertainties in α^*_R [e.g., *Quay*, 1997; *Hendricks et al.*, 2004]. Using $^{17}\Delta_{dis}$ obviates this problem. Values for k and C_{sat} are the same as those used in the calculations of N.

6.2. Modifications due to Equatorial Upwelling

[52] Systematic underestimation of net C production by the O_2 technique is possible if undersaturated upwelling waters in the mixed layer have not reached true steady state conditions. To estimate how many of our sample locations may be affected by this process, we built a simple model where initially undersaturated waters, with O_2 characteristics typical of surface waters at the equator, travel meridionally in 1-D surface flow away from the upwelling center. In this model, the O_2 properties evolve according to equation (3) and its isotopic analogs. N and G are held constant at 20 mmol O_2 m^{-2} d^{-1} (~14 mmol C m^{-2} d^{-1}) and 120 mmol O_2 m^{-2} d^{-1} (~44 mmol ^{14}C m^{-2} d^{-1}), respectively. The mixed layer depth (h) is 50 m. k is 4 m d^{-1} and C_{sat} is 200 mmol m^{-3}. In surface waters at the equator along 95°W and 110°W, C/C_{sat} = 0.9 and $^{17}\Delta_{dis}$ = 70 per meg (see Figures 1 and 2). The meridional

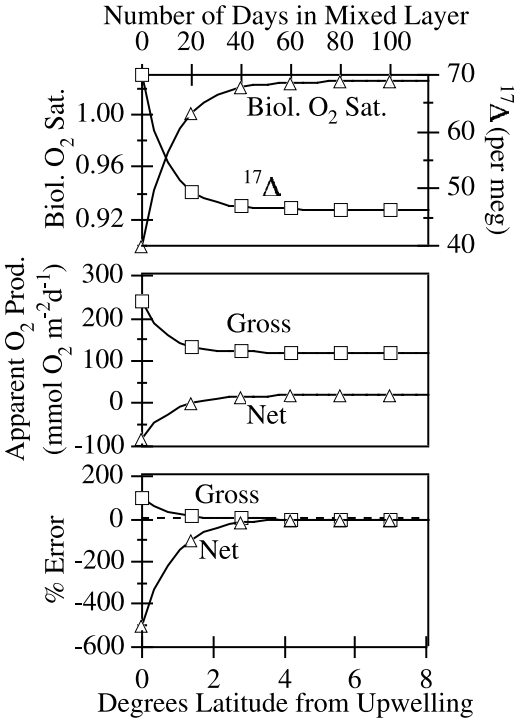

Figure 8. Results from the one-dimensional model of meridional advective transport. (top) Evolution of biological O_2 saturation and $^{17}\Delta_{dis}$ with latitude after water upwells. (middle) Steady state estimates of gross and net O_2 production rates based on the mixed layer $^{17}\Delta_{dis}$ and biological O_2 saturation. (bottom) Corresponding percent error in estimated rates of production.

advection rate is 0.07° latitude d^{-1}, the average of estimates from *Philander et al.* [1987] and *Poulain* [1993].

[53] Figure 8 shows how biological O_2 saturation increases to the steady state value of 1.022 and how $^{17}\Delta_{dis}$ decreases to the steady state value of +46 per meg. The rates of net and gross O_2 production that would be calculated based on these values are shown in Figure 8 (middle). The calculated rate of gross production reaches the true rate faster than the calculated rate of net production reaches its true rate. The apparent gross production rate is within 20% of the actual gross production rate after the water has traveled ~1° (15 days). Apparent net production does not reach 20% of the specified rate until the water has traveled 2.75° from the upwelling center (40 days). If an initial condition of $C/C_{sat} = 1$ is used instead of 0.9, the apparent net production rate is within 20% of the specified rate after 15 days, similar to the gross production rate.

[54] With these model results in mind, we look at the mixed layer biological O_2 saturation and $^{17}\Delta_{dis}$ data at 95°W and 110°W (Figure 9). Biological O_2 saturation was always less than 0.9 in the region most impacted by upwelling, between 2°S and the equator, and was less than 1 at 2°N in 5 of 6 samples. Beyond this region, biological O_2 saturation was greater than 1, except at 8°N, 95°W. At this location, upwelling of low O_2 waters associated with the NEC-NECC boundary raises the isotherms and, we believe, is responsible for the low biological O_2 saturation. The increases in $[NO_3^-]$ and $[Si(OH)_4]$ at 8°N are consistent with local upwelling. The $^{17}\Delta_{dis}$ values are similar (25–95 per meg) across the entire region, including the upwelling zones.

[55] On the basis of our model results and data we limit samples used for calculations of the net production rate and the N/G ratio to those south of 4.75°S and north of 2.75°N (outside the shaded region in the biological O_2 saturation panel of Figure 9). For calculations of the gross production rate, we limit the samples to those south of 3°S and north of 1°N (outside the shaded region in the $^{17}\Delta$ panel of Figure 9). We also neglect the point at 8°N, 95°W because this is another region of upwelling [*McClain et al.*, 2002]. Open circles in Figure 9 mark samples excluded from our net and gross calculations.

6.3. Net and Gross Production Rates

[56] In this section, we look at our rate estimates and compare our results to those of three other studies (see Table 1 for a summary): *Fiedler et al.* [1991], *Chavez et al.* [1996], and the JGOFS study in the equatorial Pacific [*Murray et al.*, 1995; *McCarthy et al.*, 1996; *Barber et al.*, 1996]. *Fiedler et al.* [1991] and *Chavez et al.* [1996] estimated rates of new production over large regions of the eastern equatorial Pacific (encompassing our lines at 95°W and 110°W) based on NO_3^- fluxes into and out of their study areas. The JGOFS work took place farther to the west, at 140°W, but is included here because there are generally few data from the equatorial Pacific. In that study, *McCarthy et al.* [1996] determined rates of new production from rates of $^{15}NO_3^-$ uptake during incubations ($\leq$4 hours in duration). All three studies relied on the same method, incubations with spiked HCO_3^- (either ^{13}C or ^{14}C), to determine rates of ^{14}C production (or primary production).

[57] In order to compare our results to those of other studies, we converted our estimates, which are in terms of O_2 production, to more common units of C production. Net O_2 production was converted to net C production using a photosynthetic quotient of 1.4 [*Laws*, 1991]. We converted from gross O_2 production to ^{14}C production by dividing gross O_2 production by 2.7 [*Marra*, 2002]. It follows that in order to compare our values for N/G O_2 production to the more common *f* ratio (defined in the other three studies as new production/^{14}C production), we multiplied N/G O_2 production by the factor of 2.7/1.4 (see above). Our estimates for rates of net C production, *f* ratio, and ^{14}C production are shown in Figure 9. Our data reflects average rates for the mixed layer (as opposed to the euphotic zone). The number of samples analyzed at each location is noted in the biological O_2 saturation panel.

[58] We begin with results for net production. The average rate of net C production from our samples was 6.9 ± 6.2 mmol C m^{-2} d^{-1} (1σ, n = 11). The range in individual uncertainties was ±0.6 mmol C m^{-2} d^{-1} (5°N, 110°W, 25m) to ±5.8 mmol C m^{-2} d^{-1} (8°S, 95°W, 10m). These uncertainties, shown in Figure 9, were based on errors of ±0.002 in biological O_2 saturation, as discussed in section 3, and an uncertainty of 30% in the gas invasion rate (kC_{sat}). Our average rates were higher south of the equator than to the north. This result is based on very few data and must be investigated further. We note that it does conform to the expected pattern, given higher nutrient burdens in the eastern equatorial Pacific south of the equator.

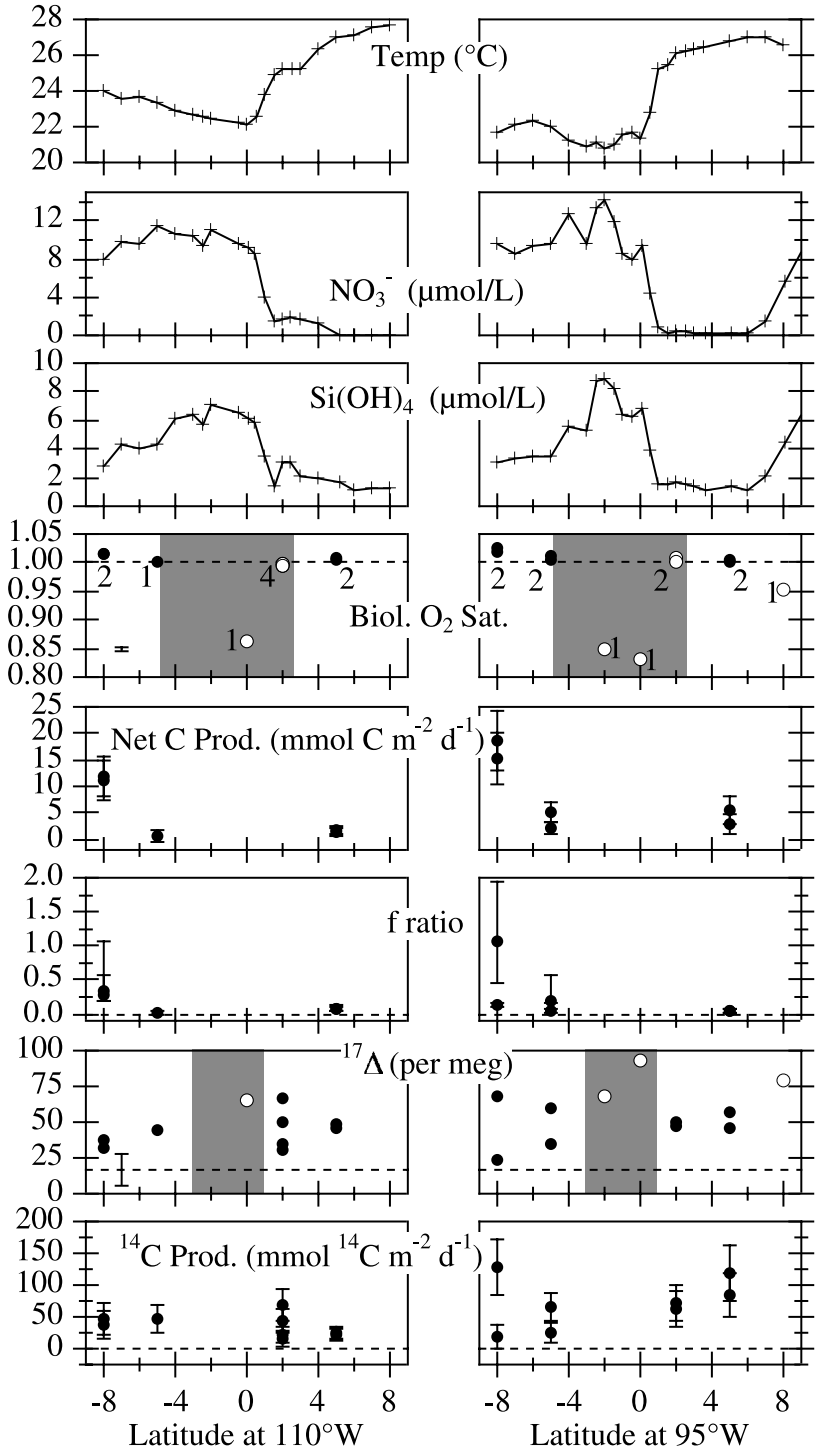

Figure 9. Chemical, isotopic, and rate data along 95°W and 110°W. Surface temperature, $[NO_3^-]$, and $[Si(OH)_4]$ measurements are from all stations along the transits. O_2 properties are from the mixed layer (squares in Figures 1a and 2a); the number of sampling depths is given in the biological O_2 saturation panel. The shaded regions are upwelling zones where active resaturation occurs. Points shown as open circles are excluded from calculations of production rates as described in the text. Error bars that represent one standard deviation from the mean of replicates are shown for the measurements of biological O_2 saturation (±0.002) and $^{17}\Delta_{dis}$ (±11 per meg). Errors in *f* ratio are calculated assuming these uncertainties in biological O_2 saturation and $^{17}\Delta_{sat}$. Errors in net C production and ^{14}C production, calculated from O_2 properties, also assume a 30% uncertainty in the gas exchange rate (kC_{sat}).

Table 1. Estimates of Production Rates in the Equatorial Pacific[a]

	This study $^{17}\Delta$ and O_2[b]	Fiedler et al. NO_3^- Fluxes and ^{14}C Incubation[c]	Chavez et al. NO_3^- Fluxes and ^{13}C Incubation[d]	JGOFS ^{15}N Incubation and ^{14}C Incubation[e]
Longitude range	95° and 110°W	95° and 110°W	90°–180°W	140°W
Net C production, mmol C m^{-2} d^{-1}	6.9 ± 6.2, 8°–5°N and 5°–8°S	10–40, 5°N–5°S	14–20, 5°N–5°S	9.9, 12°N–12°S
^{14}C production, mmol C m^{-2} d^{-1}	53 ± 34, 8°–2°N and 5°–8°S	35–65, 8°N–8°S	72 ± 12, 95° and 110°W, 5°N–5°S	52 ± 5, 10°N–10°S
f ratio	0.12 ± 0.11, 8°–5°N and 5°–8°S	0.29 ± 0.11, eastern equatorial Pacific	0.18–0.27, 5°N–5°S	0.10, 5°N–7°S

[a]All measurements of net and gross production have been converted to net C production (mmol C m^{-2} d^{-1}) and ^{14}C production, respectively, by the methods outlined in the text.
[b]Biological O_2 saturation and $^{17}\Delta$ of dissolved O_2 (this study).
[c]NO_3^- drawdown and ^{14}C incubations [*Fiedler et al.*, 1991].
[d]NO_3^- drawdown and ^{13}C incubations [*Chavez et al.*, 1996].
[e]^{15}N incubations [*McCarthy et al.*, 1996] and ^{14}C incubations [*Barber et al.*, 1996].

[59] In comparison, *Fielder et al.* [1991, Figure 13] estimated new production rates of 10–40 mmol C m^{-2} d^{-1} at locations south of ~5°N, along 95°W and 110°W. Rates of new production decreased sharply north of ~5°N. *Chavez et al.* [1996] estimated new production for the entire equatorial Pacific region from 5°N–5°S, 90°–180°W, as averaging 14–20 mmol C m^{-2} d^{-1}. *McCarthy et al.* [1996] estimated new production along 140°W (12°S–12°N) as averaging 9.9 mmol C m^{-2} d^{-1}. This value does not account for excretion of ^{15}N as DON during the experiment, which, elsewhere is ~30% of $^{15}NO_3^-$ assimilation [*Bronk and Ward*, 2000]. Given the high nutrient burden in the eastern equatorial Pacific, we expected that rates we measured would be among the highest in the region. It remains to be seen if the relatively low rates we measured are characteristic of other times.

[60] Our average ^{14}C production rate of 53 ± 34 mmol C m^{-2} d^{-1} (1σ, n = 17; individual uncertainties ranged from ±9.3 mmol C m^{-2} d^{-1} at 5°N, 110°W, 25 m to ±45.3 mmol C m^{-2} d^{-1} at 8°S, 95°W, 25 m) agrees with those of ^{14}C incubations (Table 1) from *Fiedler et al.* [1991], *Chavez et al.* [1996], and the JGOFS study [*Barber et al.*, 1996]. Our uncertainties (shown in Figure 9) are based on errors of ±11 per meg in $^{17}\Delta_{dis}$, as discussed in section 3, and 30% in the gas invasion rate (kC_{sat}). The contour map of *Fiedler et al.* [1991, Figure 7] shows ^{14}C production values in the range of 35–65 mmol C m^{-2} d^{-1} in the region of 95°–110°W, 8°S–8°N. The measurements of *Chavez et al.* [1996] yielded ^{14}C production rates of 70 ± 14 mmol C m^{-2} d^{-1} and 75 ± 20 mmol C m^{-2} d^{-1} at 95°W and 110°W, respectively. Over the region 10°S–10°N along 140°W, *Barber et al.* [1996] found ^{14}C production rates of 44 ± 4 and 59 ± 10 mmol C m^{-2} d^{-1}, during the periods February–March 1992 and August–September 1992, respectively.

[61] Our results indicate *f* ratios (Figure 9) were consistently low except at 8°S, 95°W, where we found one (impossibly) high value (*f* ratio = 1.06) associated with a very large uncertainty ($^{+0.87}_{-0.62}$). Excluding this point, our average value for the *f* ratio in the mixed layer along 95°W and 110°W was 0.12 ± 0.11 (1σ; n = 10; max uncertainty of $^{+0.73}_{-0.14}$ at 8°S, 110°W, 25m and min uncertainty of ±0.02 at 5°S, 95°W, 25 m and at 5°N, 95°W, 25 m). Uncertainties in the *f* ratio (Figure 9) were calculated assuming errors of ±0.002 in biological O_2 saturation and ±11 per meg in $^{17}\Delta_{dis}$, as discussed in section 3. *Fiedler et al.* [1991] found an average *f* ratio over the eastern Pacific of 0.29 ±0.11. This is similar to the results of *Chavez et al.* [1996]; an average *f* ratio of 0.18–0.27 over the region 90°–180°W, 5°N–5°S. *McCarthy et al.* [1996] determined a lower value of 0.10, close to ours, over the range 5°N–7°S at 140°W. Our average *f* ratio of 0.12 ± 0.11 thus agrees with the low end of the range of these other results.

[62] We note that our comparisons involve rates determined at different times and in different areas. Methodological uncertainties are always important. Excellent agreement is therefore not expected. One explanation for disagreement between results from the O_2 technique and other methods is a difference in the depth of integration. The $^{17}\Delta_{dis}$ and biological O_2 saturation measures, as applied here, reflect production rates over the depth of the mixed layer, whereas, incubation studies are generally performed over the euphotic zone (0.1 or 1% light level). Another reason for our low *f* ratio is that we cannot calculate net production close to the equator. Hence this productive zone is excluded from our estimate.

6.4. Community Respiration Fractionation Factor

[63] Using equation (3) of *Hendricks et al.* [2004], we write an expression for the ^{18}O respiration fractionation factor, α_R^{18}, in terms of N/G, C/C_{sat}, and $\delta_{dis}^{18}O$. Values for N/G came from the $^{17}\Delta_{dis}$ and O_2/Ar analyses, while C/C_{sat} and $\delta_{dis}^{18}O$ were measured. In principle, this calculation is circular, since we require a value for α_R^{18} in order to calculate N/G and gross production from $^{17}\Delta_{dis}$ measurements. In practice, however, N/G is nearly independent of this value, whereas α_R^{18} depends strongly on the value of N/G as calculated with $^{17}\Delta_{dis}$ and O_2/Ar.

[64] We determined a value for the steady state mixed layer community along 95°W and 110°W from the 11 samples used to calculate net production rates and N/G C production (see Figure 9). The average α_R^{18} was 0.979 ± 0.002 (1σ; 11 samples). This value agrees with other estimates of α_R^{18} in phytoplankton and in the euphotic zone [*Guy et al.*, 1993; *Kiddon et al.*, 1993; *Quay et al.*, 1993; *Bender and Grande*, 1987], although previous workers have

often adopted somewhat lower values [e.g., *Bender and Grande*, 1987]. Notably, this value is similar to the ^{18}O fractionation factors obtained by *Quay et al.* [1993] in the North Pacific ($\alpha_R^{18} = 0.978 \pm 0.006$) and *Hendricks et al.* [2004] in the Southern Ocean ($\alpha_R^{18} = 0.978 \pm 0.003$). This agreement for such different locations indicates there is no trend in mixed layer α_R^{18} with surface temperature or latitude. The high value helps significantly in accounting for the large value of the Dole effect ($\delta^{18}O$ difference between air O_2 and seawater H_2O), +23.5‰ [*Bender et al.*, 1994; *Hoffman et al.*, 2004].

7. Conclusions

[65] Measurements of O_2 concentration and isotopic composition contribute to our understanding of circulation and metabolic rate processes in the equatorial Pacific. Below the mixed layer, O_2 properties also provide information about the biological and mixing histories of water masses since they were last ventilated at the surface. One interesting result is that a large fraction of O_2 in the aphotic zone derives from photosynthesis, rather than air O_2. Inclusion of O_2 properties in models of the equatorial thermocline will reveal important information about photosynthesis and respiration rates in the shallow stratified waters underlying the mixed layer.

[66] Within the mixed layer, O_2 properties, coupled with measurements of wind speed, allow us to calculate biological production rates. Particular features of this technique include the fact that analysis of a single sample characterizes net and gross production in the mixed layer, the fact that O_2 ''integrates'' the production signal over a time period of $\sim$ 10 days, and that no incubation is required. Our simple steady state model is most effective in areas far from upwelling centers, where O_2 has resaturated. Simultaneous comparisons involving this technique and other methods of estimating productivity would be valuable.

[67] **Acknowledgments.** We gratefully acknowledge others who supported us in this work. We thank the crews of the NOAA research vessels, the *Ka'imimoana* and the *Ronald Brown*, especially survey technicians, Jonathan Shannahoff and Dennis Sweeney. Katrina Hoffman of MBARI collected water samples. Greg Johnson and Kristy McTaggert of NOAA/PMEL made temperature and salinity data available to us. Conversations with Matthew Reuer were valuable. Funding was provided to Princeton by NSF and NASA and to MBARI by the NASA SIMBIOS program and NOAA's Office of Global Programs.

References

Ando, K., and M. J. McPhaden (1997), Variability of surface layer hydrography in the tropical Pacific Ocean, *J. Geophys. Res.*, *102*(C10), 23,063–23,078.

Angert, A., S. Rachmilevitch, E. Barkan, and B. Luz (2003), Effects of photorespiration, the cytochrome pathway, and the alternative pathway on the triple isotopic composition of atmospheric O_2, *Global Biogeochem. Cycles*, *17*(1), 1030, doi:10.1029/2002GB001933.

Archer, D. E., T. Takahashi, S. Sutherland, J. Goddard, D. Chipman, K. Rodgers, and H. Ogura (1996), Daily, seasonal and interannual variability of sea-surface carbon and nutrient concentration in the equatorial Pacific Ocean, *Deep Sea Res., Part II*, *43*(4–6), 779–808.

Barber, R. T., M. P. Sanderson, S. T. Lindley, F. Chai, J. Newton, C. C. Trees, D. G. Foley, and F. P. Chavez (1996), Primary productivity and its regulation in the equatorial Pacific during and following the 1991–1992 El Nino, *Deep Sea Res., Part II*, *43*(4–6), 933–969.

Bender, M. L. (1990), The $\delta^{18}O$ of dissolved O_2 in seawater: A unique tracer of circulation and respiration in the deep-sea, *J. Geophys. Res.*, *95*(C12), 22,243–22,252.

Bender, M. L., and K. D. Grande (1987), Production, respiration, and the isotope geochemistry of O_2 in the upper water column, *Global Biogeochem. Cycles*, *1*, 49–59.

Bender, M. L., T. Sowers, and L. Labeyrie (1994), The Dole effect and its variations during the last 130,000 years as measured in the Vostok ice core, *Global Biogeochem. Cycles*, *8*(3), 363–376.

Benson, B. B., and D. Krause (1984), The concentration and isotopic fractionation of oxygen dissolved in fresh-water and seawater in equilibrium with the atmosphere, *Limnol. Oceanogr.*, *29*(3), 620–632.

Blunier, T., B. Barnett, M. L. Bender, and M. B. Hendricks (2002), Biological oxygen productivity during the last 60,000 years from triple oxygen isotope measurements, *Global Biogeochem. Cycles*, *16*(3), 1029, doi:10.1029/2001GB001460.

Bronk, D. A., and B. B. Ward (2000), Magnitude of dissolved organic nitrogen release relative to gross nitrogen uptake in marine systems, *Limnol. Oceanogr.*, *45*(8), 1879–1883.

Chavez, F. P., K. R. Buck, S. K. Service, J. Newton, and R. T. Barber (1996), Phytoplankton variability in the central and eastern tropical Pacific, *Deep Sea Res., Part II*, *43*(4–6), 835–870.

Christian, J. R., M. A. Verschell, R. Murtugudde, A. J. Busalacchi, and C. R. McClain (2002), Biogeochemical modelling of the tropical Pacific Ocean. I. Seasonal and interannual variability, *Deep Sea Res., Part II*, *49*, 509–543.

Coale, K. H., et al. (1996), A massive phytoplankton bloom induced by an ecosystem-scale iron fertilization experiment in the equatorial Pacific Ocean, *Nature*, *383*, 495–501.

Craig, H., and T. Hayward (1987), Oxygen supersaturation in the ocean: Biological versus physical contributions, *Science*, *235*, 199–202.

Dugdale, R. C., and F. P. Wilkerson (1998), Silicate regulation of new production in the equatorial Pacific upwelling, *Nature*, *391*, 270–273.

Emerson, S. (1987), Seasonal oxygen cycles and biological new production in surface waters of the sub-Arctic Pacific Ocean, *J. Geophys. Res.*, *92*(C6), 6535–6544.

Emerson, S., P. Quay, and P. A. Wheeler (1993), Biological productivity determined from oxygen mass-balance and incubation experiments, *Deep Sea Res., Part I*, *40*(11–12), 2351–2358.

Emerson, S., P. D. Quay, C. Stump, D. Wilbur, and R. Schudlich (1995), Chemical tracers of productivity and respiration in the subtropical Pacific Ocean, *J. Geophys. Res.*, *100*(C8), 15,873–15,887.

Fiedler, P. C., V. Philbrick, and F. P. Chavez (1991), Oceanic Upwelling and productivity in the eastern tropical Pacific, *Limnol. Oceanogr.*, *36*(8), 1834–1850.

Gardner, W. D., S. P. Chung, M. J. Richardson, and I. D. Walsh (1995), The oceanic mixed-layer pump, *Deep Sea Res., Part II*, *42*(2–3), 757–775.

Gu, D. F., and S. G. H. Philander (1997), Interdecadal climate fluctuations that depend on exchanges between the tropics and extratropics, *Science*, *275*, 805–807.

Guy, R. D., M. L. Fogel, and J. A. Berry (1993), Photosynthetic fractionation of the stable isotopes of oxygen and carbon, *Plant Physiol.*, *101*(1), 37–47.

Harper, S. (2000), Thermocline ventilation and pathways of tropical-subtropical water mass exchange, *Tellus, Ser. A*, *52*(3), 330–345.

Hendricks, M. B., M. Bender, and B. Barnett (2004), Net and gross O_2 production in the Southern Ocean from measurements of biological O_2 saturation and its triple isotope composition, *Deep Sea Res., Part I*, *51*(11), 1541–1561.

Hoffman, G., et al. (2004), A model of the Earth's Dole effect, *Global Biogeochem. Cycles*, *18*, GB1008, doi:10.1029/2003GB002059.

Johnson, G. C., B. M. Sloyan, W. S. Kessler, and K. E. McTaggart (2002), Direct measurements of upper ocean currents and water properties across the tropical Pacific during the 1990s, *Prog. Oceanogr.*, *52*(1), 31–61.

Kiddon, J., M. L. Bender, J. Orchardo, D. A. Caron, J. C. Goldman, and M. Dennett (1993), Isotopic fractionation of oxygen by respiring marine organisms, *Global Biogeochem. Cycles*, *7*(3), 679–694.

Kirkwood, D. S. (1992), Stability of solutions of nutrient salts during storage, *Mar. Chem.*, *38*, 151–164.

Kroopnick, P., and H. Craig (1972), Atmospheric oxygen—Isotopic composition and solubility fractionation, *Science*, *175*, 54–55.

Kroopnick, P., and H. Craig (1976), Oxygen isotope fractionation in dissolved-oxygen in the deep-sea, *Earth Planet. Sci. Lett.*, *32*(2), 375–388.

Lämmerzahl, P., T. Röckmann, C. A. M. Brenninkmeijer, D. Krankowshy, and K. Mauersberger (2002), Oxygen isotope composition of stratospheric carbon dioxide, *Geophys. Res. Lett.*, *29*(12), 1582, doi:10.1029/2001GL014343.

Laws, E. A. (1991), Photosynthetic quotients, new production and net community production in the open ocean, *Deep Sea Res., Part A*, *38*(1), 143–167.

Levine, N. M., J. Dunne, J. Kiddon, and M. Bender (2003), The $\delta^{18}O$ of dissolved O_2: Implications for ocean respiration and circulation, B.A. thesis, 57 pp., Princeton Univ., Princeton, N. J.

Luz, B., and E. Barkan (2000), Assessment of oceanic productivity with the triple-isotope composition of dissolved oxygen, *Science*, *288*, 2028–2031.

Luz, B., E. Barkan, M. L. Bender, M. H. Thiemens, and K. A. Boering (1999), Triple-isotope composition of atmospheric oxygen as a tracer of biosphere productivity, *Nature*, *400*, 547–550.

Marra, J. (2002), Approaches to the measurement of plankton production, in *Phytoplankton Productivity: Carbon Assimilation in Marine and Freshwater Ecosystems*, edited by P. J. L. Williams, D. N. Thomas, and C. S. Reynolds, pp. 78–108, Blackwell, Malden, Mass.

McCarthy, J. J., C. Garside, J. L. Nevins, and R. T. Barber (1996), New production along 140 degrees W in the equatorial Pacific during and following the 1992 El Nino event, *Deep Sea Res., Part II*, *43*(4–6), 1065–1093.

McClain, C. R., J. R. Christian, S. R. Signorini, M. R. Lewis, I. Asanuma, D. Turk, and C. Dupouy-Douchement (2002), Satellite ocean-color observations of the tropical Pacific Ocean, *Deep Sea Res., Part II*, *49*(13–14), 2533–2560.

McTaggart, K. E., and G. C. Johnson (2001), CTD measurements during 1999 and 2000 as part of the Global Ocean-Atmosphere-Land System (GOALS)/Pan American Climate Studies (PACS), *NOAA Data Rep. OAR PMEL-69*, 1054 pp., Pacific Mar. Environ. Lab., Seattle, Wash.

McTaggart, K. E., and G. C. Johnson (2003), CTD measurements during 2001 and 2002 as part of the TAO/TRITON Program, *NOAA Data Rep. OAR PMEL-70*, 132 pp. and CD-ROM, Pacific Mar. Environ. Lab., Seattle, Wash.

Morel, A. (1988), Optical modeling of the upper ocean in relation to its biogenous content (case I waters), *J. Geophys. Res.*, *93*, 10,749–10,768.

Murray, J. W., E. Johnson, and C. Garside (1995), A US JGOFS process study in the equatorial Pacific (EqPac)—Introduction, *Deep Sea Res., Part II*, *42*(2–3), 275–293.

Philander, S. G. H., W. J. Hurlin, and A. D. Seigel (1987), Simulation of the seasonal cycle of the tropical Pacific Ocean, *J. Phys. Oceanogr.*, *17*(11), 1986–2002.

Poulain, P. M. (1993), Estimates of horizontal divergence and vertical velocity in the equatorial Pacific, *J. Phys. Oceanogr.*, *23*(4), 601–607.

Quay, P. (1997), Was a carbon balance measured in the equatorial Pacific during JGOFS?, *Deep Sea Res., Part II*, *44*(9–10), 1765–1781.

Quay, P. D., S. Emerson, D. O. Wilbur, C. Stump, and M. Knox (1993), The $\delta^{18}O$ of dissolved O2 in the surface waters of the sub-Arctic Pacific: A tracer of biological productivity, *J. Geophys. Res.*, *98*(C5), 8447–8458.

Rodgers, K. B., B. Blanke, G. Madec, O. Aumont, P. Ciais, and J. C. Dutay (2003), Extratropical sources of equatorial Pacific upwelling in an OGCM, *Geophys. Res. Lett.*, *30*(2), 1084, doi:10.1029/2002GL016003.

Spitzer, W. S., and W. J. Jenkins (1989), Rates of vertical mixing, gas-exchange and new production—Estimates from seasonal gas cycles in the upper ocean near Bermuda, *J. Mar. Res.*, *47*(1), 169–196.

Thiemens, M. H., T. Jackson, K. Mauersberger, B. Schueler, and J. Morton (1991), Oxygen isotope fractionation in stratospheric CO_2, *Geophys. Res. Lett.*, *18*(4), 669–672.

Thiemens, M. H., T. Jackson, E. C. Zipf, P. W. Erdman, and C. Vanegmond (1995), Carbon-dioxide and oxygen-isotope anomalies in the mesosphere and stratosphere, *Science*, *270*, 969–972.

Wanninkhof, R. (1992), Relationship between wind-speed and gas-exchange over the ocean, *J. Geophys. Res.*, *97*(C5), 7373–7382.

Wanninkhof, R., R. A. Feely, D. K. Atwood, G. Berberian, D. Wilson, P. P. Murphy, and M. F. Lamb (1995), Seasonal and lateral variations in carbon-chemistry of surface-water in the eastern equatorial Pacific during 1992, *Deep Sea Res., Part II*, *42*(2–3), 387–409.

Weiss, R. F. (1970), Solubility of nitrogen, oxygen and argon in water and seawater, *Deep Sea Res.*, *17*(4), 721–735.

Wyrtki, K., and B. Kilonsky (1984), Mean water and current structure during the Hawaii-to-Tahiti Shuttle Experiment, *J. Phys. Oceanogr.*, *14*(2), 242–254.

Yung, Y. L., A. Y. T. Lee, F. W. Irion, W. B. DeMore, and J. Wen (1997), Carbon dioxide in the atmosphere: Isotopic exchange with ozone and its use as a tracer in the middle atmosphere, *J. Geophys. Res.*, *102*(D9), 10,857–10,866.

B. A. Barnett, M. L. Bender, and M. B. Hendricks, Department of Geosciences, Princeton University, Princeton, NJ 08544, USA. (melissahendricks21@yahoo.com)

F. P. Chavez, Monterey Bay Aquarium Research Institute, 7700 Sandholt Road, Moss Landing, CA 95039, USA.

P. Strutton, College of Oceanic and Atmospheric Sciences, Oregon State University, Corvallis, OR 97331, USA.